DRAFT

Proceedings of the ASME 2013 International Mechanical Engineering Congress & Exposition
IMECE2013
November 13-21, 2013, San Diego, California, USA

IMECE2013-63300

BENCHMARKING THE ACCURACY OF INERTIAL MEASUREMENT UNITS FOR ESTIMATING JOINT REACTIONS

Ryan S. McGinnis
University of Michigan
Ann Arbor, MI, USA

Jessandra Hough
University of Michigan
Ann Arbor, MI, USA

N. C. Perkins
University of Michigan
Ann Arbor, MI, USA

ABSTRACT

Newly developed miniature wireless inertial measurement units (IMUs) hold great promise for measuring and analyzing multibody system dynamics. This relatively inexpensive technology enables non-invasive motion tracking in broad applications, including human motion analysis. The second part of this two-part paper advances the use of an array of IMUs to estimate the joint reactions (forces and moments) in multibody systems via inverse dynamic modeling. In particular, this paper reports a benchmark experiment on a double-pendulum that reveals the accuracy of IMU-informed estimates of joint reactions. The estimated reactions are compared to those measured by high precision miniature (6 dof) load cells. Results from ten trials demonstrate that IMU-informed estimates of the three dimensional reaction forces remain within 5.0% RMS of the load cell measurements and with correlation coefficients greater than 0.95 on average. Similarly, the IMU-informed estimates of the three dimensional reaction moments remain within 5.9% RMS of the load cell measurements and with correlation coefficients greater than 0.88 on average. The sensitivity of these estimates to mass center location is discussed. Looking ahead, this benchmarking study supports the promising and broad use of this technology for estimating joint reactions in human motion applications.

INTRODUCTION

The annual number of total hip and knee replacement surgeries are predicted to increase by over 170% (to 572,000) and 670% (to 3.48 million), respectively by the year 2030 [1]. This alarming increase in joint replacements motivates the need for non-invasive, clinically viable methods to identify pathological lower extremity motion before joint injuries occur. One of these potential methods, inverse dynamic modeling, begins by approximating the human body as a multibody system of rigid segments connected by joints. Knowledge of the segmental kinematics, namely the angular velocity and angular acceleration of each segment and the linear acceleration of the segment's mass center, enables a solution for the reaction kinetics (i.e. forces and moments) acting at the joints provided segmental inertial properties (e.g. mass center location, mass, inertia tensor) are known [2].

The current standard for quantifying segmental kinematics is video-based motion capture (MOCAP). MOCAP is an expensive technology that employs an array of high-speed cameras calibrated to provide three-dimensional positions of a set of reflective markers attached to a subject. Markers are typically attached to a subject's skin via adhesive tape in specific locations to define bony anatomical landmarks [3]. This method is often constrained to a dedicated motion-capture laboratory and requires an operator skilled in the placement of the reflective markers as well as the collection and analysis of the resulting marker position data.

As mentioned previously, inverse dynamic modeling requires knowledge of the angular velocity and angular acceleration of each body segment in addition to the segment's mass center acceleration. Computation of these quantities from marker position data requires a differencing operation to compute segment angles and then successive numerical differentiations to compute angular velocity and angular

acceleration. Two successive differentiations are also required to compute segmental mass center acceleration. It is well established that these numerical differentiations significantly amplify small errors in the initial position data (due to measurement error, marker occlusion, skin motion, etc.), resulting in potentially large errors in the very kinematic quantities required for inverse dynamics [4,5].

The above limitations (accuracy, cost, and laboratory infrastructure) prevent widespread adoption of MOCAP as a clinically viable tool for estimating joint reactions. However, these shortcomings may be addressed by advancing an alternative technology, namely miniaturized inertial measurement units (IMUs). Miniature IMUs, which incorporate MEMS accelerometers and angular rate gyros, measure the angular velocity and linear acceleration of any rigid body to which they are attached. When deployed as a body worn sensor array, miniature IMUs directly provide the angular velocity and linear acceleration of body segments needed for inverse dynamics and require just a single derivative operation to yield the requisite angular acceleration. Thus, miniature IMU arrays have the potential to yield far more accurate kinematic data for the inverse dynamic estimates of joint reactions than (position-based) MOCAP. In addition, miniature IMU arrays are a highly portable technology that can be deployed in the clinic, workplace, or field of play and for a very small fraction of the cost of MOCAP.

Several recent studies explore the use of IMUs for inverse dynamic modeling and in (non-laboratory) environments previously inaccessible using MOCAP [6–9]. One study employs IMUs as part of the inverse dynamic analysis of the human knee joint for patients with knee osteoarthritis [6]. Estimates of the knee adduction moment during ambulatory gait are obtained using kinematic data from a shank-mounted IMU with ground reactions measured from a wearable, instrumented shoe. Moreover, this study benchmarks the adduction moment estimated using the portable technology (IMU plus instrumented shoe) with that estimated using a laboratory-based optoelectronic marker system and a floor-mounted force plate. While it is important to benchmark the accuracy of the joint reactions estimated using data from inertial sensors, the study [6] employs a gold standard (optoelectronic cameras) which inherits the inaccuracies of MOCAP in measuring the requisite segmental kinematics.

The objective of this paper is to use a precise gold standard to explore the accuracy of joint reactions estimated using miniature IMU arrays. To this end, we conduct a careful benchmarking study where the reaction forces and moments acting at the joints of a well characterized mechanical system are directly measured from embedded six degree-of-freedom force and torque sensors. The mechanical system, an instrumented double-pendulum introduced in the companion paper [10], incorporates a two-node array of miniature wireless IMUs that provide the kinematic data for inverse dynamic estimates of the joint reactions. We open with a brief description of the double pendulum from [10] and the additional instrumentation needed for this study.

METHODS

We return to the instrumented double pendulum introduced in the companion paper [10] that provides benchmark measurements of both kinematic and kinetic data. Recall that the benchmark kinematic data is provided by two high resolution (0.07 deg.) rotary optical encoders that measure the rotations across both joints. The benchmark kinetic data is provided by two high resolution load cells embedded in the two links immediately adjacent to each joint (red cylinders, Fig. 1A). In addition, the double pendulum is instrumented with two (6 dof) IMUs, one per link (blue rectangles, Fig. 1). The instrumentation is illustrated in the schematic of Fig. 1 and also visible in the photograph of Fig. 1 of [10]. A description of the load cells is provided below and descriptions of the IMUs and encoders are provided in the companion paper [10]. Analysis of the data from these instruments requires definition of the frames of reference illustrated in Fig. 1 A-C which are further defined below

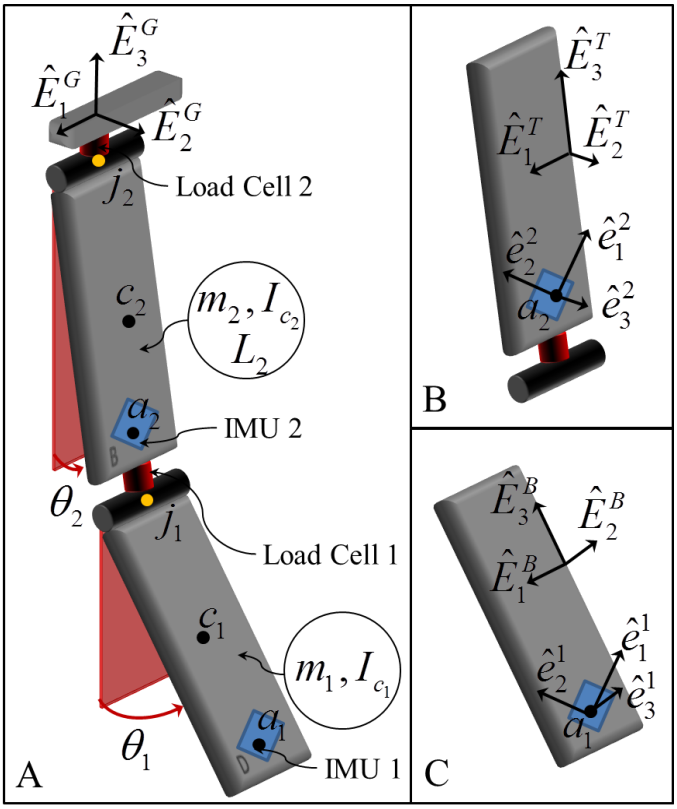

Figure 1: Schematic of the instrumented double pendulum with definitions of reference frames defined. Refer also to photograph shown in Fig. 1 of [10].

We define three reference frames to describe the dynamics of the double pendulum: frame B is fixed to the bottom link and

is composed of the orthogonal unit vectors ($\hat{E}_1^B$, $\hat{E}_2^B$, $\hat{E}_3^B$, Fig. 1C); frame T is fixed to the top link and is composed of the orthogonal unit vectors ($\hat{E}_1^T$, $\hat{E}_2^T$, $\hat{E}_3^T$, Fig. 1B); and frame G is an inertial frame composed of the unit vectors ($\hat{E}_1^G$, $\hat{E}_2^G$, $\hat{E}_3^G$, Fig. 1A). The reference frames are defined such that $\hat{E}_1^T$, $\hat{E}_1^B$, and $\hat{E}_1^G$ are parallel to the rotation axes of the links, $\hat{E}_3^B$ and $\hat{E}_3^T$ are aligned with the long axis of their respective links, and $\hat{E}_3^G$ is aligned with gravity. The link-fixed reference frames (B and T), are also assumed to be aligned with the principal axes of the links. We must also consider two additional reference frames defined by the sense axes of the two attached IMUs. The bottom link IMU reports measurements along ($\hat{e}_1^1$, $\hat{e}_2^1$, $\hat{e}_3^1$, Fig. 1C), while the top link IMU reports measurements along ($\hat{e}_1^2$, $\hat{e}_2^2$, $\hat{e}_3^2$, Fig. 1B). In general, the sense axes are not aligned with the principal axes of the links.

The two load cells noted in Fig. 1A are Nano17™ force/torque sensors which provide three-axis measurement of both force and moment. They resolve forces up to 70 N along the length of the pendulum links and 50 N in the two transverse directions, and all with a resolution of 0.0125 N. They resolve moments up to 500 N-mm about all three axes with a resolution of 0.0625 N-mm. Load cell #1, mounted to the distal end of the top link at joint j_1, measures reactions at this joint and with components resolved in frame T. Load cell #2, mounted to the support at joint j_2, measures reactions at this joint and with components resolved in frame G. The reaction forces ($\vec{F}_1$, $\vec{F}_2$) and moments ($\vec{M}_1$, $\vec{M}_2$) measured by each load cell are shown in the free body diagrams of the bottom and top links in Fig. 2A and B, respectively.

Starting from the free body diagrams in Fig. 2, systematic use of the Newton-Euler equations for each body yields expressions for the reactions. Specifically, Newton's second law for both links yields the reaction forces

$$\vec{F}_1 = m_1\left(\vec{a}_{c1} - \vec{g}\right) \quad (1)$$

$$\vec{F}_2 = \vec{F}_1 + m_2\left(\vec{a}_{c2} - \vec{g}\right) \quad (2)$$

where m_1 and m_2 is the mass of the bottom and top link, respectively, $\vec{a}_{c1}$ and $\vec{a}_{c2}$ is the acceleration of the mass center of the bottom and top link, respectively, and $\vec{g}$ denotes gravity. Similarly, Euler's second law for both links yields the reaction moments

$$\vec{M}_1 = I_{c1}\dot{\vec{\omega}}_1 + \vec{\omega}_1 \times I_{c1}\vec{\omega}_1 - \left(\vec{r}_{j1/c1} \times \vec{F}_1\right) \quad (3)$$

$$\vec{M}_2 = I_{c2}\dot{\vec{\omega}}_2 + \vec{\omega}_2 \times I_{c2}\vec{\omega}_2 - \left(\vec{r}_{j2/c2} \times \vec{F}_2\right) + \vec{M}_1 + \left(\vec{r}_{j1/c2} \times \vec{F}_1\right) \quad (4)$$

where I_{c1} and I_{c2} is the inertia tensor (principal axes through centroid) for the bottom and top links, respectively, $\vec{r}_{j1/c1}$ is a position vector locating j_1 relative to the (bottom link) mass center c_1, $\vec{r}_{j1/c2}$ and $\vec{r}_{j2/c2}$ are position vectors locating j_1 and j_2 relative to the (top link) mass center c_2, respectively, and $\vec{\omega}_1$, $\dot{\vec{\omega}}_1$, $\vec{\omega}_2$, and $\dot{\vec{\omega}}_2$ denote the angular velocity and angular acceleration of the bottom and top link, respectively.

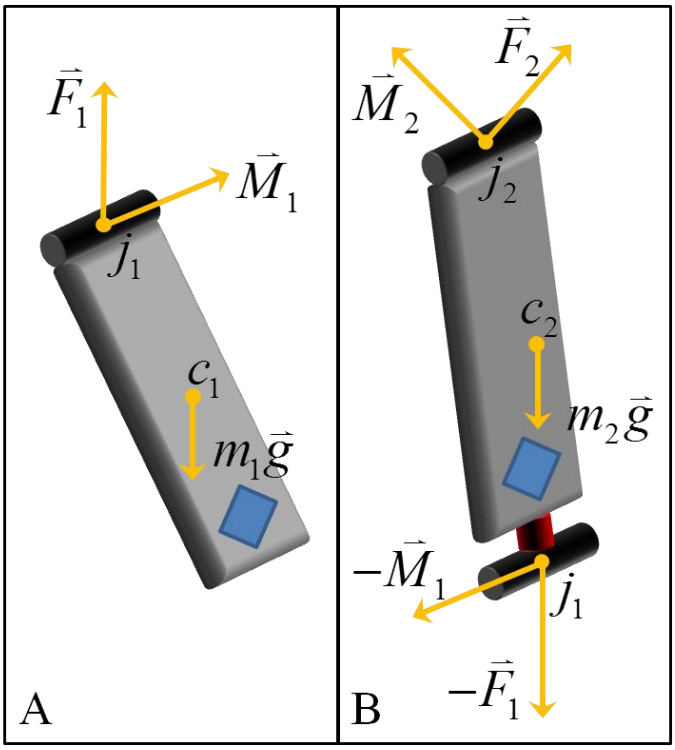

Figure 2: Free body diagrams for the bottom (A) and top (B) link of the double pendulum.

Solving (1)-(4) in sequence yields solutions for the joint reactions assuming knowledge (measurement) of all kinematical quantities, the link geometry and inertia properties. Table 1 reports the dimensions, mass, and principal moments of inertia for each link. The link dimensions and mass are measured directly, while principal moments of inertia are estimated by approximating each link as a rectangular prism of constant density with the dimensions and mass noted in the table.

Parameter	Bottom	Top
Length (m)	0.305	0.356
Width (m)	0.051	0.051
Height (m)	0.019	0.019
Mass (kg)	0.834	0.908
I_1 (kg-m^2)	0.007	0.010
I_2 (kg-m^2)	0.007	0.010
I_3 (kg-m^2)	<0.001	<0.001

Table 1: Summary of dimensions, mass and principal moments of inertia for each link.

The kinematical quantities are measured or estimated from IMU data for the freely decaying pendular motion described in [10]. The IMU provides direct measurement of link angular velocity ($\vec{\omega}_1$, $\vec{\omega}_2$) and thus link angular acceleration ($\dot{\vec{\omega}}_1$, $\dot{\vec{\omega}}_2$) following numerical differentiation. The IMU also measures the acceleration at the center of the accelerometer polluted by gravity [1]. Conveniently, gravitational pollution in the measured acceleration is canceled by the weight forces appearing in (1) and (2). However, solution of (2) and (4), and direct comparison of the calculated reactions to load cell measurements requires knowledge of the orientation of each link relative to frame G.

The orientation of each link is found from the orientation of the attached IMU and in two steps. The first step establishes the initial orientation of the IMU sense axes when the pendulum is in equilibrium. The second step determines the change in orientation upon integrating the link angular velocity during the subsequent oscillations.

During the first step, the pendulum hangs at rest. The accelerometers measure solely the acceleration due to gravity thus establishing the initial direction of $\hat{E}_3^G$ in each IMU frame of reference. Next, the pendulum is displaced from equilibrium, released and oscillates freely with decaying amplitude. The angular velocity measured by the angular rate gyros establishes the orientation of the axis of rotation $\hat{E}_1^G$ which remains fixed relative to the IMU frames. The average direction of the angular velocity is used to deduce the direction of $\hat{E}_1^G$ with respect to both IMU frames. Finally, the initial orientation of $\hat{E}_2^G$ resolved in the IMU frames follows from $\hat{E}_2^G = \hat{E}_3^G \times \hat{E}_1^G$. The initial direction cosine matrices, R, that define the orientation of the IMU frames, ($\hat{e}_1^1$, $\hat{e}_2^1$, $\hat{e}_3^1$) and ($\hat{e}_1^2$, $\hat{e}_2^2$, $\hat{e}_3^2$), relative to frame G ($\hat{E}_1^G$, $\hat{E}_2^G$, $\hat{E}_3^G$) follow immediately from the components of $\hat{E}_1^G$, $\hat{E}_2^G$ and $\hat{E}_3^G$ established by this procedure. The components of each direction cosine matrix also establishes the initial values of the Euler parameters $(\varepsilon_1, \varepsilon_2, \varepsilon_3, \varepsilon_4)$ per

$$R = \begin{bmatrix} \varepsilon_1^2 - \varepsilon_2^2 - \varepsilon_3^2 + \varepsilon_4^2, & 2(\varepsilon_1\varepsilon_2 - e_3 e_4), & 2(\varepsilon_1\varepsilon_3 + \varepsilon_2\varepsilon_4) \\ 2(\varepsilon_1\varepsilon_2 + e_3 e_4), & \varepsilon_2^2 - \varepsilon_1^2 - \varepsilon_3^2 + \varepsilon_4^2, & 2(\varepsilon_2\varepsilon_3 - \varepsilon_1\varepsilon_4) \\ 2(\varepsilon_1\varepsilon_3 - \varepsilon_2\varepsilon_4), & 2(\varepsilon_2\varepsilon_3 + \varepsilon_1\varepsilon_4), & \varepsilon_3^2 - \varepsilon_1^2 - \varepsilon_2^2 + \varepsilon_4^2 \end{bmatrix} \quad (5)$$

for subsequent use in the second step.

During the second step, the evolution of the Euler parameters from the initial condition above is governed by the differential equation

$$\begin{bmatrix} \dot{\varepsilon}_1 \\ \dot{\varepsilon}_2 \\ \dot{\varepsilon}_3 \\ \dot{\varepsilon}_4 \end{bmatrix} = \frac{1}{2} \begin{bmatrix} 0 & \omega_3(t) & -\omega_2(t) & \omega_1(t) \\ -\omega_3(t) & 0 & \omega_1(t) & \omega_2(t) \\ \omega_2(t) & -\omega_1(t) & 0 & \omega_3(t) \\ -\omega_1(t) & -\omega_2(t) & -\omega_3(t) & 0 \end{bmatrix} \begin{bmatrix} \varepsilon_1 \\ \varepsilon_2 \\ \varepsilon_3 \\ \varepsilon_4 \end{bmatrix} \quad (6)$$

where ω_1, ω_2, and ω_3 are the three components of the measured angular velocity. This ordinary differential equation is integrated forward in time using standard numerical integration techniques subject to the Euler parameter normalization constraint $\varepsilon_1^2 + \varepsilon_2^2 + \varepsilon_3^2 + \varepsilon_4^2 = 1$ at each time step. Doing so provides the Euler parameters as functions of time during the subsequent oscillations of the pendulum and therefore the orientation of the top and bottom links.

Small errors in rate gyro calibration and sensitivity to temperature subject the Euler parameters to an accumulation of error over time known as drift [11,12]. One can correct for drift by fusing accelerometer and rate gyro derived estimates of orientation via a Kalman or complementary filter [11,12]. In this study, we instead exploit the constraint that the pendulum oscillates about its equilibrium position to correct for drift. In particular, the Euler parameters must also oscillate about their initial (equilibrium) values.

The direction cosine matrix $R_1(t)$ defines the orientation, at every instant in time, of the bottom link IMU measurement frame to the G frame according to

$$\vec{v}\big|_G = R_1(t)\,\vec{v}\big|_{\hat{e}_1^1, \hat{e}_2^1, \hat{e}_3^1} \quad (7)$$

where $\vec{v}\big|_G$ is a generic vector resolved in the G frame and $\vec{v}\big|_{\hat{e}_1^1, \hat{e}_2^1, \hat{e}_3^1}$ is the same generic vector resolved in the bottom link IMU measurement frame. An analogous direction cosine matrix, $R_2(t)$, is developed for the top link. Note that $R_1(0)$ and $R_2(0)$ also define the constant orientation of the bottom link IMU measurement frame to frame B and the top link IMU measurement frame to frame T, respectively.

[1] The MEMS accelerometers measure acceleration down to zero Hertz and therefore measure gravity in addition to the superimposed acceleration due to movement.

Having defined the orientations of each IMU relative to gravity, we then use IMU data to define the mass center acceleration of each link, polluted by gravity, according to

$$\vec{a}_{c1} = \vec{a}_{m1} + \dot{\vec{\omega}}_1 \times \vec{r}_{c1/a1} + \vec{\omega}_1 \times \left(\vec{\omega}_1 \times \vec{r}_{c1/a1}\right) \quad (8a)$$

$$\vec{a}_{c2} = \vec{a}_{m2} + \dot{\vec{\omega}}_2 \times \vec{r}_{c2/a2} + \vec{\omega}_2 \times \left(\vec{\omega}_2 \times \vec{r}_{c2/a2}\right) \quad (8b)$$

where $\vec{a}_{m1}$ and $\vec{a}_{m2}$ is the acceleration measured by the bottom and top link accelerometers, respectively, and $\vec{r}_{c1/a1}$ and $\vec{r}_{c2/a2}$ are position vectors locating the mass center of the bottom and top links relative to their respective accelerometers. These position vectors are unknown and, in practice, difficult to determine. However, these unknown position vectors can be written as the sum of two vectors that are easier to determine. For the bottom link, consider that

$$\vec{r}_{c1/a1} = \vec{r}_{j1/a1} + \vec{r}_{c1/j1} \quad (9)$$

where $\vec{r}_{j1/a1}$ is the position of j_1 relative to the accelerometer, and $\vec{r}_{c1/j1}$ is the position of the link mass center relative to the joint. In human subject studies, $\vec{r}_{c1/j1}$ is often estimated from anthropometric data (or an alternative approach [13]) and $\vec{r}_{j1/a1}$ is estimated based on methods like those presented in [14]. In this study, a coordinate measuring machine (MicroScribe G2x, positional accuracy/resolution of 0.23/0.13 mm) is used to measure $\vec{r}_{j1/a1}$, and $\vec{r}_{c1/j1}$ is initially approximated as locating the geometric center of the link.

Finally, to compare the joint reactions estimated from (1)-(4) to the load cell-measured values, we first need to resolve both in a common frame of reference. Details of this procedure are presented in Annex A.

RESULTS AND DISCUSSION

The experiment and methods described above provide IMU-based estimates of joint reactions for direct comparison with those measured by embedded load cells. This section presents a series of results that benchmark the accuracy of the IMU-based estimates. We open by reviewing IMU data for an example trial. We demonstrate the accuracy of the calculated link orientation through comparisons with the link angles measure by the optical encoders. We then present the IMU-estimated joint reactions, based on the initial assumption that the link mass centers coincide with their geometric centers. We then relax that assumption in arriving at superior estimates of the joint reactions.

Figure 3 illustrates the IMU data for the bottom link during a free oscillation test as described in [10]. Three components of acceleration (Fig. 3A) and angular velocity (Fig. 3B) are plotted as functions of time, where the blue, green, and red curves correspond to data resolved along the $\hat{e}_1^1$, $\hat{e}_2^1$, and $\hat{e}_3^1$ sense axes, respectively.

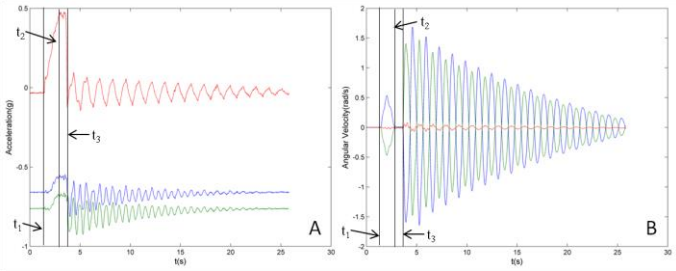

Figure 3: IMU acceleration (A) and angular velocity (B) history for an example trial sampled from the bottom link IMU. The pendulum begins at rest in its stable equilibrium position ($t < t_1$), is perturbed from this position by hand ($t_1 < t < t_2$) and then released ($t = t_3$).

The behavior of the pendulum during this trial is immediately discernible in Fig. 3. Specifically, the pendulum remains at rest in its stable equilibrium position ($t < t_1$), is perturbed from this position by hand and held stationary ($t_2 < t < t_3$), and released ($t = t_3$) and allowed to oscillate freely about equilibrium ($t > t_3$). Note that the accelerometer measures the acceleration due to gravity at the start of the trial while the pendulum is at rest. As described above, we exploit this fact to determine the initial orientation of the IMU frames prior to subsequent integration of (6). This integration provides the (drift-polluted) estimate of the orientation of each link throughout the remainder of the trial. Figure 4 illustrates the uncorrected (drift-polluted) estimates of the four Euler parameters for the bottom link (gray curves) as well as their drift corrected values (colored curves) from the start of the example trial until 10 seconds after t_3.

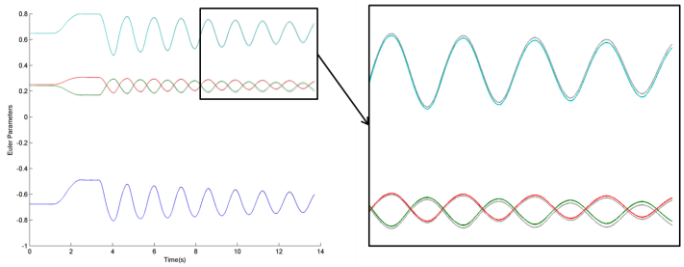

Figure 4: Drift polluted (gray) and corrected (colored) Euler parameters defining the orientation of the bottom link up until 10 seconds after t_3 during the example trial.

While the difference between the corrected and drift polluted Euler parameters during the first 10 seconds of oscillation is quite modest, the drift correction ensures that each Euler parameter oscillates about its initial value as required by the periodic motion of the pendulum. We confirm the accuracy of the corrected Euler parameters by using them to construct the angle formed by the major axis of each link ($\hat{E}_3^B$ and $\hat{E}_3^T$) and gravity ($\hat{E}_3^G$). As described in [10], these angles are also measured by the optical encoders which provide the truth data for comparison with the IMU-based estimates. The mean and

standard deviation of the root mean squared error (RMSE) and the correlation coefficient (r) between the encoder-measured and IMU-calculated angles for all ten trials are reported in Table 2. A similar analysis, assuming planar motion, is presented in [10]. The results confirm that link orientation based on integrating IMU data remains an excellent estimate of the true orientation as directly measured by the encoders (RMSE $\leq$ 1.6 deg. and r $\geq$ 0.998).

	Bottom		Top	
Parameter	RMSE (deg)	r	RMSE (deg)	r
Mean (SD)	1.54 (0.24)	1.00 (<0.001)	0.87 (0.22)	1.00 (<0.001)

Table 2: Mean and standard deviation of root mean square error (RMSE) and correlation coefficient (r) between IMU-calculated link angles and encoder-measured link angles for all ten trials.

Having established the accuracy of the IMU-derived orientation estimates, we evaluate the accuracy of IMU-derived estimates of joint reactions. We first present the calculated reactions at j_2 upon assuming the mass centers of the links are collocated with their geometric centers. For the same trial above, the three components of load cell measured force (Fig. 5A) and moment (Fig. 5B) are shown as dashed curves while the IMU derived force and moment are shown as the solid curves. The blue, green, and red curves correspond to reactions resolved along the $\hat{E}_1^G$, $\hat{E}_2^G$, and $\hat{E}_3^G$ directions, respectively.

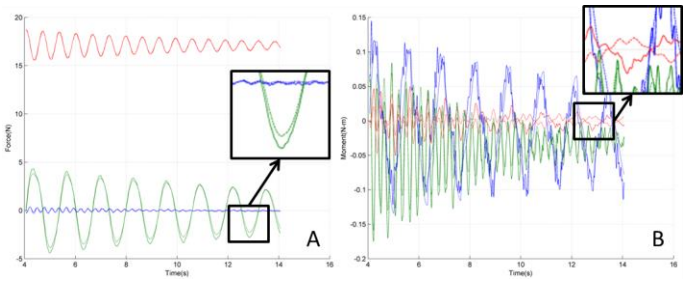

Figure 5: Reaction force (A) and moment (B) at j_2 as measured by the load cells (dashed) and estimated using IMU data (solid). The three colors distinguish components resolved in frame G: blue= $\hat{E}_1^G$, green= $\hat{E}_2^G$, and red= $\hat{E}_3^G$.

The agreement in the three components of force is outstanding and it is difficult to discern differences between the IMU-based estimates (solid curves) and the load cell measurements (dashed curves) on this scale. For example, the $\hat{E}_2^G$ component (green curve) of the predicted reaction force has the maximum root mean squared error (RMSE) of only 3.3% relative to the weight of the top link. By contrast, there are discernible differences between the IMU predicted moment components and those measured by the load cell. The difference is particularly observable for the moment acting about the vertical ($\hat{E}_3^G$) axis (see red curve in Fig 5B for $10 \leq t \leq 14$ s for example) which has an RMSE of 3.0% relative to the restoring moment acting on the top link at the start of the trial.

For further comparison, we normalize the force components by the weight of each link and the moment components by the initial restoring moment due to the weight of each link at the moment of release. After normalization, the non-dimensional force and moment components estimated using IMU data are plotted against those measured by the load cell. The resulting plots, after subtracting the mean of each component, are illustrated in Figure 6. The blue, green and red curves again distinguish components along the $\hat{E}_1^G$, $\hat{E}_2^G$, and $\hat{E}_3^G$ directions, respectively.

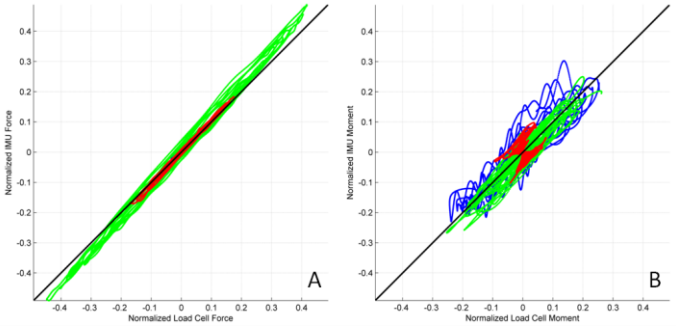

Figure 6: Three components of normalized force (A) and moment (B) acting at j_2 as predicted by IMU-enabled inverse dynamic modeling plotted against those measured directly by the load cell. The three colors distinguish components resolved in frame G: blue= $\hat{E}_1^G$, green= $\hat{E}_2^G$, and red= $\hat{E}_3^G$.

Figures 6A and 6B illustrate the resulting force and moment comparison, respectively. For reference, the black line has zero intercept and unit slope. These results reinforce the excellent agreement between the estimated and measured reaction force components, each of which have correlation coefficient exceeding 0.90. As suggested in Fig. 5B, however, there is less agreement between the estimated and measured reaction moment components. In particular, the correlation coefficient is as small as 0.21 for one moment component ($\hat{E}_3^G$ direction) for this trial. Table 3 summarizes the results for all ten trials by reporting the mean (standard deviation) of the correlation coefficient (r) and the root mean square error (RMSE) as a percentage of normalizing factor between the estimated and measured reactions at both joint j_1 and joint j_2.

Joint	j_1					
	$\vec{F}_1$			$\vec{M}_1$		
Direction	$\hat{E}_1^T$	$\hat{E}_2^T$	$\hat{E}_3^T$	$\hat{E}_1^T$	$\hat{E}_2^T$	$\hat{E}_3^T$
% RMSE	0.51 (0.09)	1.92 (0.39)	0.60 (0.16)	1.12 (0.19)	0.81 (0.19)	0.17 (0.02)
r	0.96 (0.03)	0.99 (0.01)	1.00 (<0.01)	0.96 (0.01)	0.98 (0.01)	0.87 (0.07)
Joint	j_2					
	$\vec{F}_2$			$\vec{M}_2$		
Direction	$\hat{E}_1^G$	$\hat{E}_2^G$	$\hat{E}_3^G$	$\hat{E}_1^G$	$\hat{E}_2^G$	$\hat{E}_3^G$
% RMSE	0.76 (0.13)	4.61 (0.84)	1.16 (0.37)	6.38 (1.37)	3.61 (0.74)	3.19 (0.14)
r	0.95 (0.03)	1.00 (<0.01)	1.00 (<0.01)	0.88 (0.04)	0.97 (0.02)	0.58 (0.25)

Table 3: Mean (standard deviation) of RMS difference (RMSE) and correlation coefficient (r) for IMU-derived force and moment components compared to those measured by the load cells at j_1 and j_2. Results are for the 10 trials based on assuming the mass centers are at the geometric centers of the links.

The results in Table 3 demonstrate that IMU-based estimates of the force components remain within 4.7% RMS of measured values (relative to the weight of each link) and have correlation coefficients greater than 0.95 on average. In contrast, the estimated moment components remain within 6.4% RMS of measured values (as compared to the initial restoring moment acting on each link) and have correlation coefficients greater than 0.58. Possible error sources include small errors in the physical properties of each link (mass, mass center, moment of inertia, etc.), small misalignment errors between the measured and IMU-derived force and moment components, and small IMU calibration errors.

Principal among these errors sources is the known sensitivity to small errors in mass center position [3,15]. To investigate this, the mass center position of each link is now experimentally estimated. We begin with the procedure in [10] which assumes that the mass center of a link lies along the major axis. The location along that axis is then estimated from measurements of the natural frequencies of the decoupled and coupled links; refer to estimates of l_1 and l_2 in [10]. In addition, we also experimentally measure potential "transverse" components of the mass center along the minor and intermediate principal axes. The two transverse components are estimated from (1) and (2) by employing force measurement from the load cells and kinematic measurements from the optical encoders. To this end, we rewrite (1) and (2) in terms of the absolute link angular velocities and accelerations ($\vec{\omega}_1$, $\vec{\omega}_2$, $\dot{\vec{\omega}}_1$, $\dot{\vec{\omega}}_2$) determined from successive differentiations of the encoder data, arriving at

$$\vec{F}_1 = m_1\left[\dot{\vec{\omega}}_2 \times \vec{r}_{j1/j2} + \vec{\omega}_2 \times \left(\vec{\omega}_2 \times \vec{r}_{j1/j2}\right) + \dot{\vec{\omega}}_1 \times \vec{r}_{c1/j1} + \vec{\omega}_1 \times \left(\vec{\omega}_1 \times \vec{r}_{c1/j1}\right) - \vec{g}\right] \quad (10)$$

$$\vec{F}_2 = \vec{F}_1 + m_2\left[\dot{\vec{\omega}}_2 \times \vec{r}_{c2/j2} + \vec{\omega}_2 \times \left(\vec{\omega}_2 \times \vec{r}_{c2/j2}\right) - \vec{g}\right] \quad (11)$$

Here, $\vec{F}_1$ and $\vec{F}_2$ are the reaction forces measured by the load cells, $\vec{r}_{j1/j2}$ is the location of j_1 relative to j_2 as measured using the coordinate measuring machine, and $\vec{r}_{c1/j1}$ and $\vec{r}_{c2/j2}$ are the two unknown center of mass locations Equations (10) and (11) are formed at each time step during an example trial and $\vec{r}_{c1/j1}$ and $\vec{r}_{c2/j2}$ are found using standard least squares. From this analysis, the new mass center locations are

$$\vec{r}_{c1/j1} = \left[-0.001,\ 0.0027,\ -0.1522\right] \quad (12)$$

$$\vec{r}_{c2/j2} = \left[-0.0233,\ -0.0111,\ -0.1891\right] \quad (13)$$

This updated estimate of mass center locations represents a 0.9% and 7.9% change from the previously assumed geometric centers of the bottom and top link, respectively, relative to the length of each link.

This seemingly small update, however, produces a significant change in the reaction moment predicted via inverse dynamic modeling as evidenced by the results of Fig.7. Figure 7 illustrates the predicted and measured force and moment components at j_1 (Fig. 7A/B) and j_2 (Fig. 7C/D) for the same trial considered above.

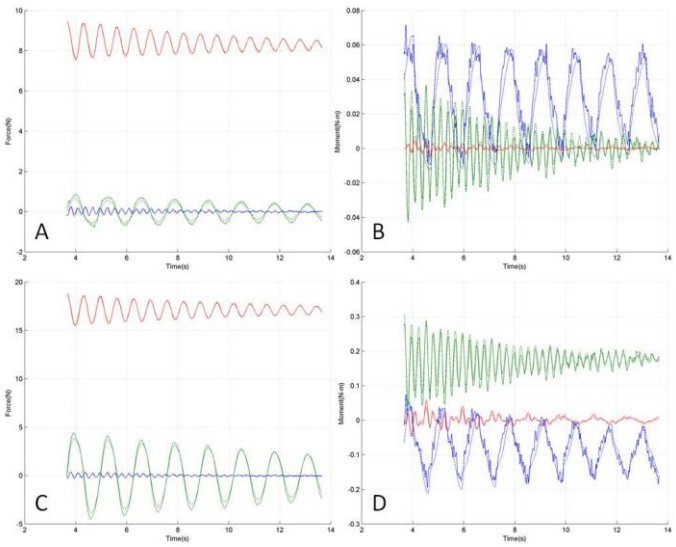

Figure 7: Force (A) and moment (B) components at j_1 and force (C) and moment (D) components at j_2 using updated mass center positions. Solid curves correspond to IMU-predicted reactions while dashed curves correspond to load cell measurements. The three colors distinguish components resolved in frame G: blue= $\hat{E}_1^T$, $\hat{E}_1^G$, green= $\hat{E}_2^T$, $\hat{E}_2^G$, and red= $\hat{E}_3^T$, $\hat{E}_3^G$.

The three components of load cell measured force (Fig. 7A/C) and moment (Fig. 7B/D) are shown as dashed curves

while the IMU-derived force and moment components are shown as solid curves. The reactions at j_1 are presented in Fig. 7A/B, where the blue, green, and red curves correspond to reactions resolved along the $\hat{E}_1^T$, $\hat{E}_2^T$, and $\hat{E}_3^T$ directions, respectively. The reactions at j_2 presented in Fig. 7C/D can be compared directly to the results presented in Figure 5. Qualitatively, the agreement between estimated and measured reaction force components remains excellent while agreement between the estimated and measured moment components is considerably improved. In particular, the maximum RMSE among all three estimated force components at j_2 decreases to 2.1% for this trial. Similarly, the RMS error in the $\hat{E}_3^T$ component of the reaction moment decreases to 1.4% (red curve, 3.0% initially).

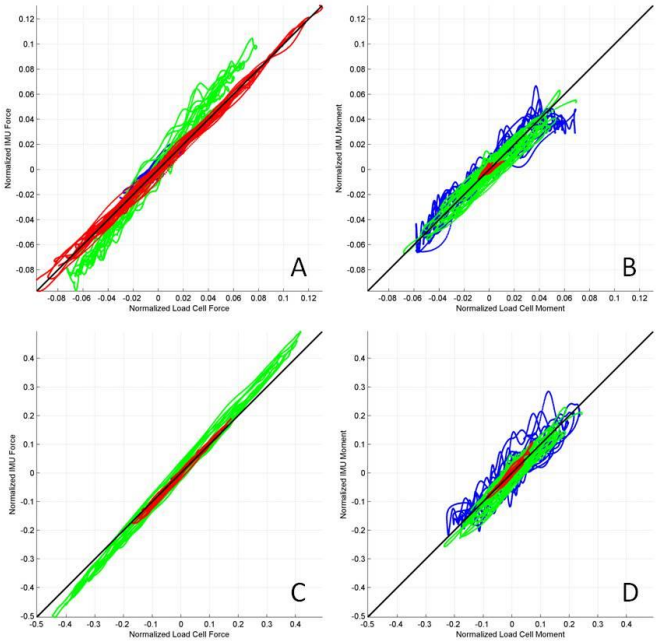

Figure 8: Normalized force (A) and moment (B) components at j_1 and normalized force (C) and moment (D) at j_2 using updated mass center positions. Estimated values are plotted versus measured values.

A systematic comparison is provided in Fig. 8 which shows normalized predicted force and moment components plotted against their measured values (again subtracting the mean from each component). The three components of normalized predicted force (Fig. 8A/C) and moment (Fig. 8B/D) are plotted against those measured by the load cell at j_1 (Fig. 8A/B) and j_2 (Fig. 8C/D). Comparison of the results in Fig. 8B and D with Fig. 6 B and D reveals a qualitative improvement in agreement between moment components. Specifically, the minimum correlation between the predicted and measured components of reaction moment at j_2 increases from 0.22 to 0.75. In contrast, the minimum correlation between the predicted and measured reaction force components at j_2 remains essentially unchanged. Table 4 summarizes the results of all ten trials including the mean (SD) RMS error and correlation coefficient.

Joint	j_1					
	$\vec{F}_1$			$\vec{M}_1$		
Direction	$\hat{E}_1^T$	$\hat{E}_2^T$	$\hat{E}_3^T$	$\hat{E}_1^T$	$\hat{E}_2^T$	$\hat{E}_3^T$
% RMSE	0.51 (0.09)	1.92 (0.40)	0.61 (0.19)	1.18 (0.21)	0.81 (0.19)	0.19 (0.03)
r	0.96 (0.03)	0.99 (0.01)	1.00 (<0.01)	0.95 (0.02)	0.98 (0.01)	0.84 (0.07)
Joint	j_2					
	$\vec{F}_2$			$\vec{M}_2$		
Direction	$\hat{E}_1^G$	$\hat{E}_2^G$	$\hat{E}_3^G$	$\hat{E}_1^G$	$\hat{E}_2^G$	$\hat{E}_3^G$
% RMSE	0.77 (0.14)	4.99 (0.85)	1.23 (0.37)	5.83 (1.22)	3.25 (0.69)	0.99 (0.21)
r	0.95 (0.023)	1.00 (<0.01)	1.00 (<0.01)	0.88 (0.04)	0.98 (0.02)	0.97 (0.01)

Table 4: Mean (standard deviation) of RMS difference (RMSE) and correlation coefficient (r) for IMU-derived force and moment components compared to those measured by the load cells at and for the 10 trials using the updated mass center location.

As reported in Table 4, the estimated force components remain within 5.0% RMS of their measured values (again normalized by the weight of each link) and exhibit correlation coefficients greater than 0.95 on average. Moreover, the estimated moment components remain within 5.8% RMS of their measured values (again normalized by the initial restoring moments) and exhibit correlation coefficients greater than 0.84 on average. Thus, the updated mass center position significantly increases the average correlation coefficient from 0.58 (the original mass center location) to 0.84. This represents a substantial improvement from a seemingly minor change (less than 8% of the length of the link) in mass center location, a finding consistent with prior human motion studies employing MOCAP [3,5,15,16]. In this experiment, however we demonstrate this sensitivity as compared to a precise gold standard (embedded load cells) and for a well characterized (mechanical) multi-body system. In human motion studies, these conditions no longer exist. Often, mass center location is estimated from anthropometric data, which can be inaccurate [17], and human body segments have a degree of flexibility that manifests in variable locations of both mass center and center/axis of rotation [18,19]. The agreement herein between the IMU estimated reactions and load cell measured reactions represent a limiting case that demonstrates a reasonable upper-bound accuracy for this technique.

CONCLUSION

This paper summarizes results from a careful experiment that benchmarks the use of IMU arrays for estimating reaction forces and moments acting at the joints of a simple multi-body system; namely a double pendulum. These predicted reactions are compared to reactions measured directly by precision miniature force and torque sensors. Results for 10 trials demonstrate that IMU-enabled inverse dynamic modeling estimates all components of reaction forces to within 5.0% RMS of their measured values (relative to the weight of each link) and with correlation coefficients greater than 0.95 on average. Similarly, the estimated components of the reaction moments remain within 5.9% RMS of their measured values (relative to the restoring moment due to the weight of each link) and with correlation coefficients greater than 0.84 on average. We highlight the sensitivity of the predicted moments to errors in mass center location. In particular, accurate estimates of reaction moments require very accurate estimates of mass center location (on the order of 8% or less of the length of the links in this experiment). These limitations aside, the results of this paper also point to the future use of wireless IMU arrays for estimating the reactions at the major skeletal joints of the human body in supporting injury prevention and rehabilitation, athlete and soldier performance, among numerous other possible uses.

ACKNOWLEDGMENTS

This material is based upon work supported by the National Science Foundation through NSF Graduate Research Fellowships awarded to J. H. and R. M.

REFERENCES

[1] Kurtz S., Ong K., Lau E., Mowat F., and Halpern M., 2007, "Projections of primary and revision hip and knee arthroplasty in the United States from 2005 to 2030," JBJS, **89**(4), pp. 780–785.

[2] Winter D. A., 1990, Biomechanics and motor control of human movement, Wiley, New York.

[3] Langenderfer J. E., Laz P. J., Petrella A. J., and Rullkoetter P. J., 2008, "An efficient probabilistic methodology for incorporating uncertainty in body segment parameters and anatomical landmarks in joint loadings estimated from inverse dynamics," J Biomech Eng, **130**(1), p. 014502.

[4] Davy D. T., and Audu M. L., 1987, "A dynamic optimization technique for predicting muscle forces in the swing phase of gait," Journal of Biomechanics, **20**(2), pp. 187–201.

[5] Riemer R., Hsiao-Wecksler E. T., and Zhang X., 2008, "Uncertainties in inverse dynamics solutions: A comprehensive analysis and an application to gait," Gait & Posture, **27**(4), pp. 578–588.

[6] Van den Noort J. C., van der Esch M., Steultjens M. P. M., Dekker J., Schepers H. M., Veltink P. H., and Harlaar J., 2012, "The knee adduction moment measured with an instrumented force shoe in patients with knee osteoarthritis," Journal of Biomechanics, **45**(2), pp. 281–288.

[7] Krüger A., McAlpine P., Borrani F., and Edelmann-Nusser J., 2012, "Determination of three-dimensional joint loading within the lower extremities in snowboarding," Proc Inst Mech Eng H, **226**(2), pp. 170–175.

[8] Rouhani H., Favre J., Crevoisier X., and Aminian K., 2011, "Ambulatory measurement of ankle kinetics for clinical applications," J Biomech, **44**(15), pp. 2712–2718.

[9] Faber G. S., Kingma I., and van Dieën J. H., 2010, "Bottom-up estimation of joint moments during manual lifting using orientation sensors instead of position sensors," J Biomech, **43**(7), pp. 1432–1436.

[10] Hough J., McGinnis R. S., and Perkins N. C., 2013, "Benchmark of IMU derived kinetic energy via double pendulum," Proceedings of ASME 2013 International Mechanical Engineering Congress and Exposition, San Diego, CA.

[11] Savage P., 2000, Strapdown analytics, Strapdown Associates, Maple Plain, MN.

[12] Titterton D. H., and Weston J. L., 2004, Strapdown inertial navigation technology, Institution of Electrical Engineers, Stevenage, UK.

[13] Dillon M. P., Barker T. M., and Pettet G., 2008, "Effect of inaccuracies in anthropometric data and linked-segment inverse dynamic modeling on kinetics of gait in persons with partial foot amputation," Journal of Rehabilitation Research and Development, **45**(9), pp. 1303–16.

[14] McGinnis R. S., and Perkins N. C., "Inertial Sensor Based Method for Identifying Ball Joint Center of Rotation," Journal of Biomechanics, **Submitted**.

[15] Reinbolt J. A., Haftka R. T., Chmielewski T. L., and Fregly B. J., 2007, "Are patient-specific joint and inertial parameters necessary for accurate inverse dynamics analyses of gait?," IEEE Trans Biomed Eng, **54**(5), pp. 782–793.

[16] Holden J. P., and Stanhope S. J., 1998, "The effect of variation in knee center location estimates on net knee joint moments," Gait & Posture, **7**(1), pp. 1–6.

[17] Rao G., Amarantini D., Berton E., and Favier D., 2006, "Influence of body segments' parameters estimation models on inverse dynamics solutions during gait," Journal of Biomechanics, **39**(8), pp. 1531–1536.

[18] Cole G., Nigg B., van den Bogert A., and Gerritsen K., 1996, "Lower extremity joint loading during impact in running," Clinical Biomechanics, **11**(4), pp. 181–193.

[19] Pain M. T. G., and Challis J. H., 2006, "The influence of soft tissue movement on ground reaction forces, joint

torques and joint reaction forces in drop landings," Journal of Biomechanics, **39**(1), pp. 119–124.

ANNEX A

INVERSE DYNAMICS EQUATIONS

In this annex we present the equations used to calculate the reaction force and moment acting at each joint of the double pendulum from IMU data for comparison to load cell measurements. The reactions at j_1, resolved in frame T, are defined as

$$\vec{F}_1\big|_T = m_1 R_2^T R_1 \Big[\vec{a}_{m1} + \dot{\vec{\omega}}_1 \times R_1^T(0)\vec{r}_{c1/a1} + \vec{\omega}_1 \times \big(\vec{\omega}_1 \times R_1^T(0)\vec{r}_{c1/a1}\big)\Big] \tag{14}$$

$$\vec{M}_1\big|_T = R_2^T R_1 R_1^T(0)\Big[I_{c1}\big(R_1(0)\dot{\vec{\omega}}_1\big) + \big(R_1(0)\vec{\omega}_1\big) \times I_{c1}\big(R_1(0)\vec{\omega}_1\big) - \vec{r}_{j1/c1} \times \big(R_1^T R_2 \vec{F}_1\big|_T\big)\Big] \tag{15}$$

where $\bullet\big|_T$ refers to a vector resolved in frame T, $R_1(0)$ is the (constant) direction cosine matrix defining the orientation of the bottom link IMU measurement frame relative to frame B, and the other variables are as defined in the body of the paper. The reaction force and moment at j_2, resolved in frame G, are defined as

$$\vec{F}_2\big|_G = R_2\Big[R_2^T(0)\vec{F}_1\big|_T + m_2\big(\vec{a}_{m2} + \dot{\vec{\omega}}_2 \times R_2^T(0)\vec{r}_{c2/a2} + \vec{\omega}_2 \times \big(\vec{\omega}_2 \times R_2^T(0)\vec{r}_{c2/a2}\big)\big)\Big] \tag{16}$$

$$\vec{M}_2\big|_G = R_2\Big[I_{c2}R_2(0)\dot{\vec{\omega}}_2 + R_2(0)\vec{\omega}_2 \times I_{c2}R_2(0)\vec{\omega}_2 - \vec{r}_{j2/c2} \times \vec{F}_2\big|_T + \vec{M}_1\big|_T + \vec{r}_{j1/c2} \times \vec{F}_1\big|_T\Big] \tag{17}$$

where $\bullet\big|_G$ refers to a vector resolved in frame G, $R_2(0)$ is the direction cosine matrix that defines the orientation of the top link IMU measurement frame relative to frame T, and the other variables are as defined in the body of the paper. The reaction force and moment defined in (14)-(17) are compared directly to the measured force and moment at each joint in the Results and Discussion section included above.

